Kovove Mater. 60 2022 341–349
DOI: 10.31577/km.2022.5.341

Effect of boron addition on microstructure and toughness of Ti-containing weld metals

Bingxin Wang*, Jing Li

College of Mechanical Engineering, Liaoning Shihua University, Fushun 113001, China

Received 23 February 2022, received in revised form 11 June 2022, accepted 8 September 2022

Abstract

Ti-containing weld metals with boron (B) contents of 0–85 ppm were prepared, and the microstructural characteristics and impact toughness of weld metals were investigated. The results show that compared with the weld metal without B, in the weld metal with 22 ppm B, the fraction of acicular ferrite (AF) is increased from 26 to 76 %, accompanied by a remarkable decrease in the contents of pro eutectoid ferrite (PF), grain boundary ferrite (GBF) and side-plate ferrite (SPF). In the 39 ppm B weld metal, the microstructure basically consists of AF. However, a further increase in the B content up to 61 ppm decreases the fraction of AF to 66 % due to the formation of bainitic ferrite (BF). For the weld metal with 85 ppm B, the microstructure is wholly composed of BF. The size of martensite-austenite (M/A) islands distributed between AF plates is much smaller, and the amount is much lower than this between BF plates. In the case of the weld metals primarily composed of AF, during fracture of impact specimens, crack propagation deflects much more frequently in comparison to the weld metals with large amounts of PF, GBF and SPF, or BF, which improves the toughness of weld metals. The coarse M/A islands readily induce microcracks at the interface between M/A islands and the ferrite matrix, deteriorating the toughness. The weld metals with B contents of 22 and 39 ppm exhibit outstanding impact toughness because of a high fraction of AF accompanied by fine M/A islands.

K e y w o r d s: weld metal, boron content, hardenability, acicular ferrite, toughness

1. Introduction

The microstructures of low carbon low alloy steel weld metals are usually composed of different amounts of coarse-grained transformation products (i.e., PF, GBF and SPF), BF, and fine AF constituents, depending on the chemical compositions of weld metals, welding processes, cooling conditions, etc. The microstructural constituent type plays a substantial role in determining the mechanical properties, especially the toughness of weld metals. Compared with other ferrite morphology constituents, such as PF, GBF and SPF, AF can significantly enhance the toughness of weld metals owing to its fine-grained and chaotically arranged microstructural characteristics [1–3]. Therefore, AF is desirable to develop extensively in the weld metal microstructures.

AF nucleates intragranularly in the form of independent plates on the inclusions [4], so the inclusion feature is a crucial factor affecting AF formation. The literature [5–8] reported that some specific types of Ti-containing inclusions could effectively promote AF nucleation by Mn depletion and/or crystallographic lattice match mechanisms. In addition, the hardenability of weld metal also has a considerable effect on the AF formation [9] as a result of the competitive relationships between AF and PF, GBF, SPF, etc., in the course of the austenite decomposition during cooling after welding [10]. The formation temperatures for PF, GBF and SPF are higher than that for AF [11], and, as a result, PF, GBF and SPF are precipitated before AF during austenite to ferrite transformation under lower hardenability of weld metal [12]. For the sake of a high proportion of AF in the microstructure and desirable mechanical properties, by addition of appropriate alloy elements, the hardenability of weld metal is

*Corresponding author: tel.: +86 24 56863067; e-mail address: wangbingxin@163.com

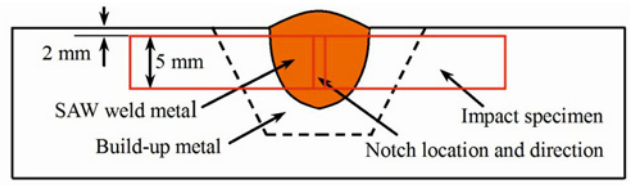

Fig. 1. Preparations of the experimental weld metal and impact specimen.

increased to suppress coarse transformation products of PF, GBF and SPF. Mosallaee et al. [2] studied the influence of Ni content on the microstructure and mechanical properties in E7018-G electrode weld metal. They pointed out that when Ni is increased to a critical content of 1.2 wt.%, the fraction of AF is enhanced from 32 to 62 %, accompanied by decreased amounts of PF, GBF and SPF. Accordingly, yield and tensile strengths, as well as impact toughness of weld metal, are improved noticeably. Winarto et al. [3] obtained similar conclusions about microstructure and impact toughness relationship for different Ni levels of an electrode in multi-pass FCA welded SM570-TMC steel joints. Additionally, expected microstructures and mechanical properties are obtained by adding Mo or Cr elements [13] or increasing Mn content [14] in weld metals.

Boron element is another additive used to increase the hardenability, and even a small amount of B can enhance the hardenability of weld metal. Free B dissolved in austenite is known to segregate strongly to the austenite grain boundaries, lowering the interfacial energy. Based on the transformation thermodynamics, the decrease in the interfacial energy raises the energy barrier for ferrite nucleation at the austenite grain boundaries and, as a result, suppresses the transformation products preferentially nucleated at prior austenite grain boundaries, such as PF, GBF and SPF [15–18]. Consequently, the hardenability of weld metal and/or steel is enhanced [19, 20].

In the present study, the weld metals with different B contents were prepared by a submerged arc welding process. Moreover, a certain amount of Ti was added to form Ti-containing inclusions, which can effectively promote AF nucleation. In these weld metals, expensive elements, such as Ni and Mo, were not added. The microstructures in the weld metals with different B contents were analyzed, and microstructure-toughness relationships were investigated.

2. Methods and materials

Figure 1 illustrates the preparation processes of experimental weld metal and impact specimens. By a plasma arc build-up welding process, pure Fe powder was first deposited in a trapezoid slot with about 15 mm depth machined in 20 mm thick C-Mn steel plates with a chemical composition (wt.%) of Fe-0.14C-0.5Si-1.55Mn-0.025S-0.022P. Subsequently, a 7 mm deep single-side V-groove was machined at the build-up welds. Finally, a single pass submerged-arc welding process in conjunction with H08MnA welding wire of 4 mm in diameter was used in the case of the voltage of 30 V and electric current of 460 A, and experimental weld metals were obtained. The compositions of the weld metals were adjusted by adding different amounts of B-Fe powder (21 % B) and a certain amount of Ti-Fe powder (33 % Ti) to the groove before welding. Furthermore, a small amount of Mn-Fe powder (81 % Mn) was filled due to very low Mn content in welding wire.

Table 1. Chemical compositions of the welding wire (mass%)

C	Mn	Si	S	P	Al
0.05	0.86	0.06	0.022	0.02	0.01

Table 2. Chemical compositions of weld metals (mass%)

C	Mn	Si	S	P	Al	Ti	B	O	N
0.062	1.55	0.25	0.028	0.035	0.015	0.021	0	380	70
0.056	1.53	0.27	0.024	0.033	0.012	0.019	22	390	68
0.061	1.58	0.19	0.027	0.031	0.015	0.022	39	385	69
0.053	1.49	0.22	0.031	0.028	0.011	0.024	61	395	67
0.058	1.52	0.26	0.022	0.032	0.013	0.021	85	400	73

(B, O, and N: in ppm)

The compositions of weld metals were determined by Shimadzu OES-5500 optical emission spectrometer except for oxygen and nitrogen, which were analyzed using a Leco TC-436 N/O analyzer. The compositions of the welding wire and weld metals are listed in Tables 1 and 2, respectively.

The specimens for metallographic microstructure observation were cut from the weld metals, and the examined planes were vertical to the welding direction. After mechanical polishing, the specimens were etched with 4 % nital solution and LePera reagent. The microstructural morphologies and M/A islands were examined under a Leica DMIRM image analyzer, and the fractions of microstructural constituents were measured.

According to Fig. 1, sub-size Charpy V-notch impact specimens ($5 \times 10 \times 55\,\mathrm{mm}^3$) were extracted from the welding joints, and impact tests were performed at –30° by the SANTAM STM-300J machine. The average values of absorbed impact energy were calculated after testing five specimens.

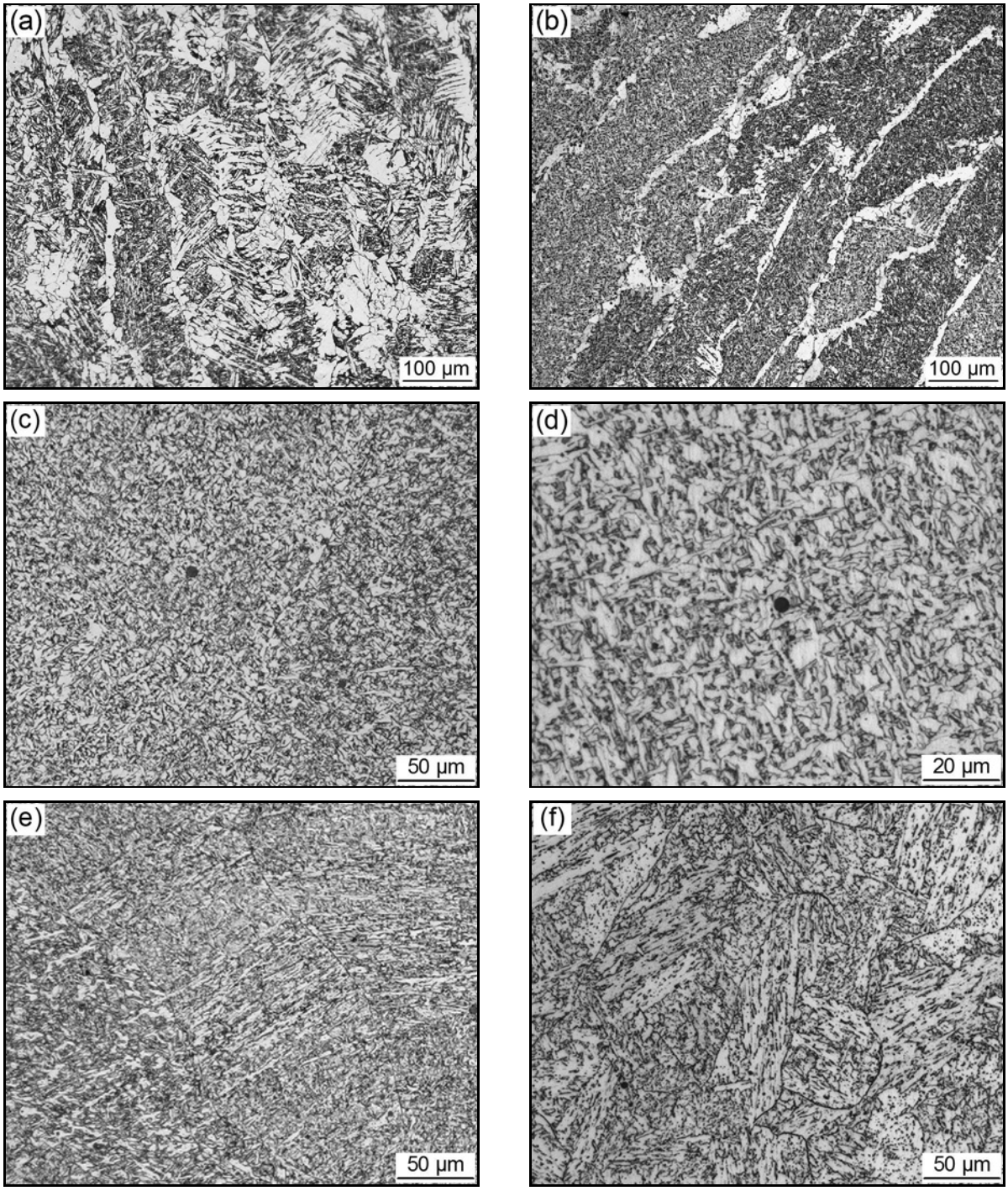

Fig. 2. Metallographic microstructures of weld metals with different B contents: (a) without B, (b) 22 ppm, (c) 39 ppm, (d) local amplification of (c) for clear observation, (e) 61 ppm, and (f) 85 ppm.

The fracture surface and the cross-sectional region beneath the fracture surface coated by nickel were observed using an FEI Quanta 600 SEM to investigate the fracture morphology and crack propagation during fracture.

3. Results and discussion

Figure 2 shows the metallographic microstructures in weld metals with different B contents, and Table 3 indicates the quantitative results of microstructural constituents. It is evident that B content has a significant effect on the weld metal microstructures.

Table 3. Quantitative measurements of constituents of weld metal microstructures

B contents	Constituents fractions (area %)			
	PF + GBF	SPF	AF	BF
without B	39	35	26	0
22 ppm	20	4	76	0
39 ppm	0	0	100	0
61 ppm	0	0	66	34
85 ppm	0	0	0	100

For the weld metal without B, the microstructure is composed of a series of different ferrite morphologies constituents, i.e., PF and GBF (39 % content), SPF (35 % content), and AF (26 % content). It is worth noting that these ferrite morphologies have a distinct difference in terms of grain size. AF constituent, as opposed to other ferrite morphologies, is much fine-grained. In the case of 22 ppm B content, the AF amount is increased to 76 %; accordingly, the fractions of PF + GBF and SPF are decreased to 20 and 4 %, respectively. In the 39 ppm B weld metal, the microstructure basically consists of AF, while other ferrite morphologies almost disappear. However, a further increase of B content to 61 ppm results in the appearance of BF with 34 % content, accompanied by a drop of AF amount to 66 %. For the weld metal with 85 ppm B, the microstructure is wholly composed of BF.

Additionally, the B element also affects the amount and size of M/A islands in the microstructures. The characteristics of M/A islands etched in the LePera reagent are shown in Fig. 3, in which M/A islands distributed between ferrite plates and ferrite matrix exhibit white and grey color characteristics, respectively. Combining with Figs. 2c and 2f, it can be seen from Fig. 3 that in the 39 ppm B weld metal (microstructure is dominated by AF), M/A islands have a tiny size and small amount, while M/A islands indicate opposite characteristics in the weld metal with 85 ppm B content (microstructure is characterized by BF).

Different ferrite morphology constituents form at their specific temperature ranges during continuous cooling in the microstructures of low-carbon steel weld metals. The formation temperatures for PF, GBF and SPF are higher than those for AF [11], while BF precipitates at a lower temperature compared with AF [21]. B element strongly enhances the hardenability of steels and/or weld metals, and reduces the austenite-to-ferrite transformation temperature [19, 20]. In the case of present compositions of weld metals, the hardenability of weld metal without B should be lower, so the austenite transforms into large amounts of PF,

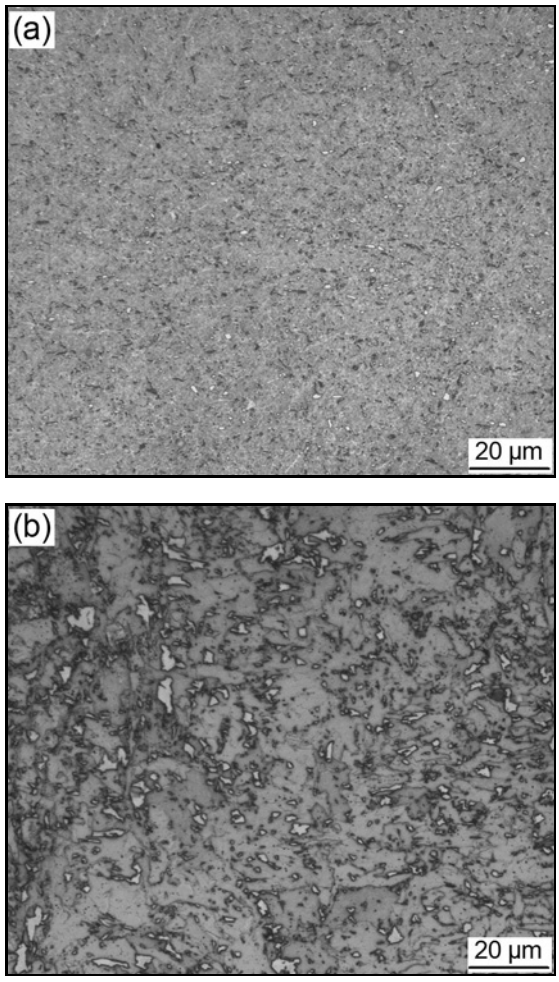

Fig. 3. M/A islands characteristics in the weld metals with B contents of (a) 39 ppm, and (b) 85 ppm.

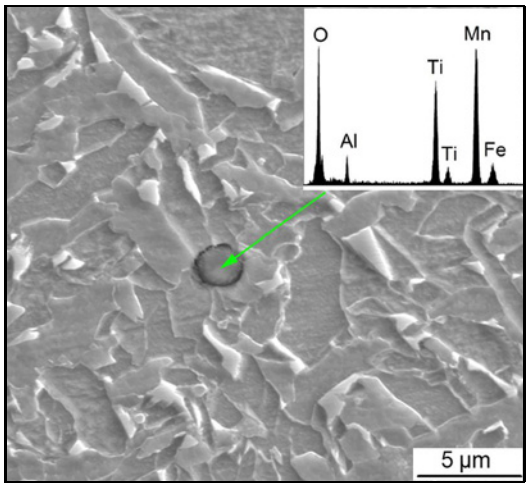

Fig. 4. SEM image of 39 ppm B weld metal microstructure, showing the promotion role of inclusion for AF nucleation.

GBF and SPF at higher temperature ranges. In the weld metals with B contents of 22 and 39 ppm, the

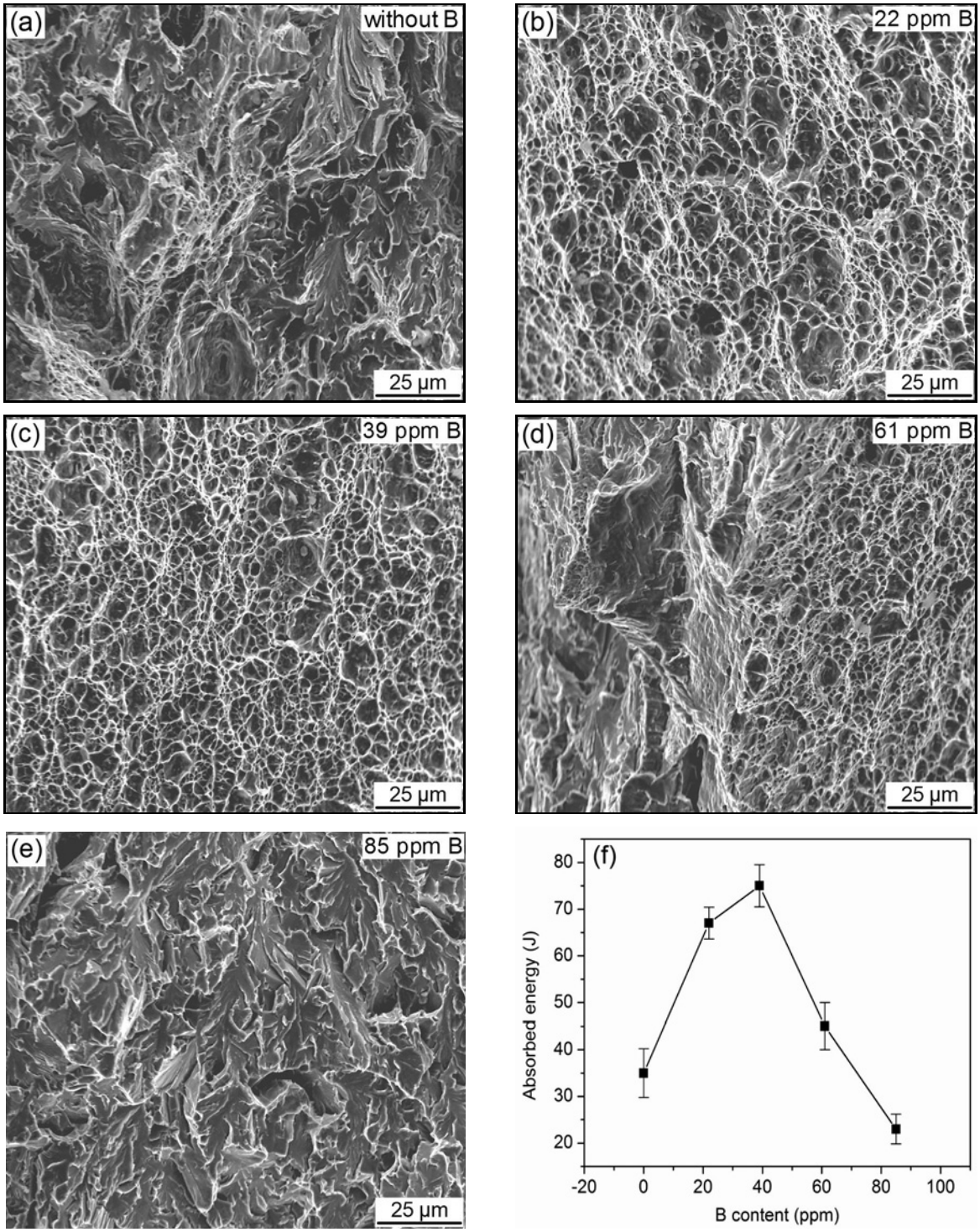

Fig. 5. Experimental results of impact test at –30°: (a)–(e) fracture morphologies and (f) impact absorbed energy.

hardenability is increased, suppressing the formation of PF, GBF and SPF, and lowering the austenite to ferrite transformation temperature. In the meantime, as shown in Fig. 4, under induced nucleation of containing-Ti inclusion for AF, AF well develops, leading to a remarkable increase in AF amount. For 61 and 85 ppm B weld metals, the hardenability is high enough to cause the decomposition of austenite to bainite at sufficiently lower temperatures. Moreover, high B content increases the austenite stability and, as a result, a large amount of M/A islands with much coarse size appear in the microstructure.

Figure 5 indicates the experimental results of the impact test for weld metals with different B contents.

For the weld metal without B, it can be seen that in addition to a small amount of dimples, a large amount of cleavage patterns are observed in the fracture surface, and the impact absorbed energy of 35 J is lower. In the case of B contents of 22 and 39 ppm, the fracture characteristics are changed from a mixture of cleavage pattern and dimple to a fully dimpled morphology. The impact absorbed energy values are markedly increased in these weld metals, especially in 39 ppm B weld metal, and the highest impact absorbed energy with 75 J is obtained. However, a further increase in the B content up to 61 ppm makes impact absorbed energy decrease to 45 J. The fracture morphology is basically the same as that of weld metal without B, except for more dimples amount in the weld metal with a B content of 61 ppm. In the weld metal with a B content of 85 ppm, the fracture morphology exhibits completely a cleavage mode with the lowest impact absorbed energy (23 J).

The impact toughness of weld metal is closely correlated with the weld metal microstructure. It is visible from the comparative analyses of Figs. 2 and 5 that for the weld metals with different B contents, the impact toughness of weld metal is enhanced gradually with the increase in AF amount in the microstructure.

Figure 6 shows the effect of microstructure on the crack propagation path during specimen fracture. It can be seen that in the case of the microstructure containing large amounts of coarse PF, GBF and SPF (weld metal without B), or the microstructure mainly composed of BF (85 ppm B weld metal), the crack propagation path is relatively straight. In contrast, crack propagation deflects for a high fraction of AF microstructure (39 ppm B weld metal).

AF is known to consist of fine-grained and chaotically arranged lath-like ferrite separated by the grain boundaries with the misorientation of 15° or more (i.e., high-angle grain boundary) [22–24]. High-angle grain boundaries (HAGBs) can efficiently hinder crack propagation, forcing crack to change propagation direction during fracture [25]. Therefore, as shown in Fig. 6b, AF can deflect crack propagation frequently due to its microstructure and grain boundary characteristics. For BF, low angle grain boundaries distribute between parallel arranged bainitic ferrite plates within a bainite packet with HAGBs [26]. Thus, the crack propagates almost in a straight line manner inside a coarse bainite packet, and the crack propagation direction does not deflect until it encounters bainite packet boundaries, as shown in Fig. 6c. Similar to BF, low-angle grain boundaries exist between adjacent side-plate ferrites [27], which can not prevent crack propagation. Although there are HAGBs between PF [28], the crack propagation also displays a straighter path due to coarse grain, as shown in Fig. 6a.

Frequently deflecting the crack paths resulting from the impediment of HAGBs can consume more

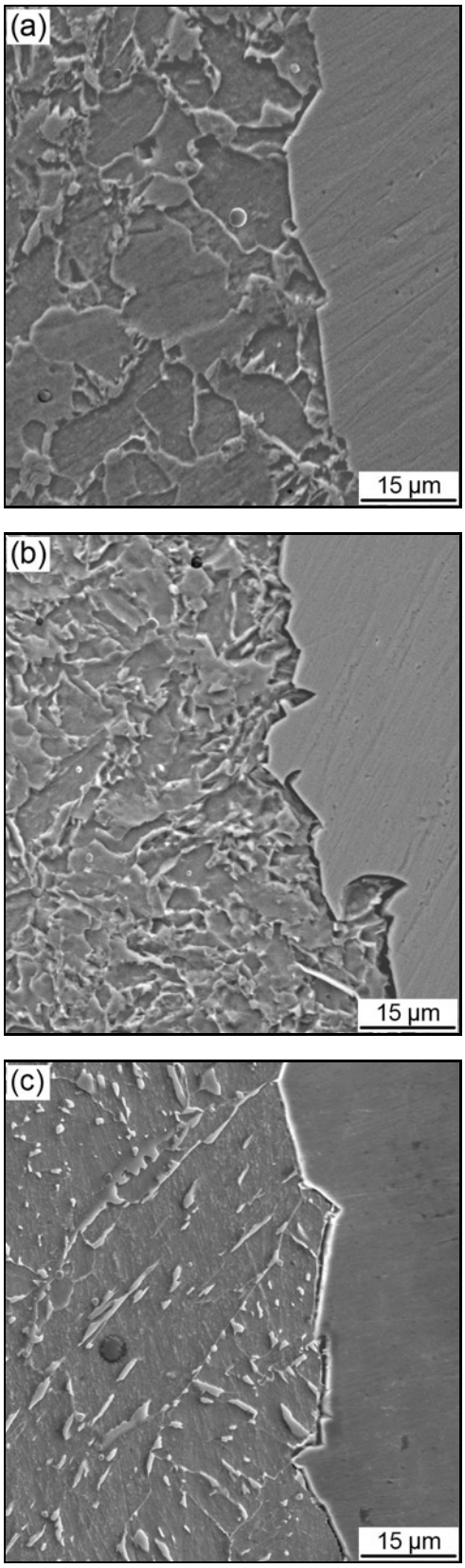

Fig. 6. SEM images of the side surfaces of the fracture surfaces for the impact specimens (a) without B, (b) with 39 ppm B, and (c) with 85 ppm B.

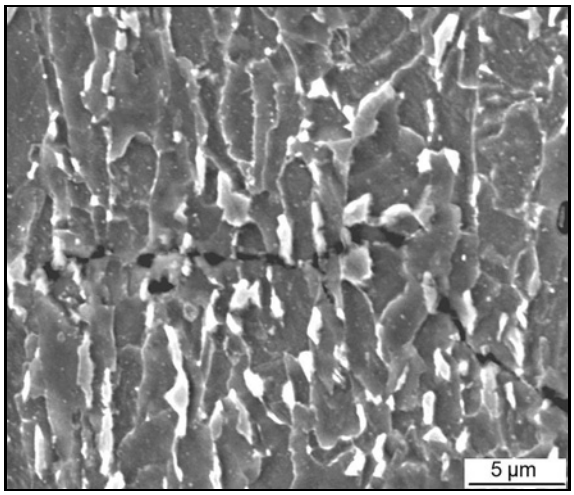

Fig. 7. SEM analysis of cross-sectional area beneath fracture surface for the impact specimen with 85 ppm B.

crack propagation energy during crack propagation, leading to an improved impact toughness [25]. Consequently, the high fraction of AF in the microstructure can increase the impact toughness of weld metal.

Furthermore, M/A islands in the microstructure also significantly affect impact toughness. Figure 7 presents that voids or microcracks usually initiate at the interfaces between coarse-sized M/A islands and ferrites, deteriorating impact toughness. Conversely, fine M/A islands hardly cause microcracks. The literature [29, 30] showed that the hard M/A islands in the soft ferrite matrix could lead to a high-stress concentration at the interfaces between M/A islands and ferrites under exerted load due to the distinctions of hardness and strength between these two structures, which readily induces microcracks. The size of M/A islands is a key factor for the microcracks formation induced by M/A islands [31, 32]. With the increase in the size of M/A islands, the exerted load for inducing the microcrack is decreased [33–35]. On the other hand, the literature [36–38] documented that fine-sized M/A islands did not impair the toughness of metal. As a consequence, the microstructures with high fraction AF, for example, 39 ppm B weld metal, exhibit outstanding impact toughness due to the small amount of M/A islands with fine size (as shown in Fig. 3a). On the contrary, for the microstructure characterized by BF, for instance, 85 ppm B weld metal, the impact toughness is deteriorated dramatically because of a large amount of coarse M/A islands (as shown in Fig. 3b).

4. Conclusions

(1) Compared with the weld metal without B, in the weld metal with 22 ppm B, the fraction of AF is increased from 26 to 76 %, accompanied by a remarkable decrease in the contents of PF, GBF and SPF. In the 39 ppm B weld metal, the microstructure basically consists of AF. However, a further increase in the B content up to 61 ppm decreases the fraction of AF to 66 % due to the formation of BF. For the weld metal with 85 ppm B, the microstructure is wholly composed of BF. The size of M/A islands distributed between AF plates is much smaller, and the amount is much lower than this between BF plates.

(2) In the case of the weld metals primarily composed of AF, crack propagation deflects much more frequently in comparison to the weld metals with large amounts of PF, GBF and SPF, or BF. The coarse M/A islands readily induce microcracks at the interface between M/A islands and the ferrite matrix, deteriorating the toughness.

(3) The weld metals with B contents of 22 and 39 ppm exhibit excellent impact toughness because of a high fraction of AF and fine M/A islands in the microstructures.

Acknowledgements

This work was financially supported by a Project of the Education Department of Liaoning Province (grant no. L2016132). The authors are grateful to Drs. H. Y. Wu and W. N. Zhang (State Key Laboratory of Rolling & Automation of Northeastern University, China) for providing help in SEM analysis works.

References

[1] L. Zhang, Y. J. Li, J. Wang, Q. L. Jiang, Effect of acicular ferrite on cracking sensibility in the weld metal of Q690+Q550 high strength steels, ISIJ Int. 51 (2011) 1132–1136. https://doi.org/10.2355/isijinternational.51.1132

[2] M. Mosallaee, M. T. Semiromi, Effect of nickel content on the microstructural, mechanical and corrosion behavior of E7018-G electrode weld metal, J. Mater. Eng. Perform. 30 (2021) 8901–8912. https://doi.org/10.1007/s11665-021-06100-9

[3] W. Winarto, H. Oktadinata, E. S. Siradj, D. Priadi, A. S. Baskoro, K. Ito, Microstructure and impact toughness relationship for different nickel level of electrode in multi-pass FCA welded SM570-TMC steel joint, Quarterly Journal of the Japan Welding Society 38 (2020) 154s–158s. https://doi.org/10.2207/qjjws.38.154s

[4] R. A. Ricks, P. R. Howell, G. S. Barritte, The nature of acicular ferrite in HSLA steel weld metals, J. Mater. Sci. 17 (1982) 732–740. https://doi.org/10.1007/BF00540369

[5] K. Uto, K. Nakayama, Y. Kisaka, F. Kimura, H. Terasaki, A study on the acicular ferrite formation in steel weld metals for gas metal arc welding, Quarterly

Journal of the Japan Welding Society 38 (2020) 6s–10s. https://doi.org/10.2207/qjjws.38.6s
[6] C. J. Zhang, L. N. Gao, L. G. Zhu, Effect of inclusion size and type on the nucleation of acicular ferrite in high strength ship plate steel, ISIJ Int. 58 (2018) 965–969. https://doi.org/10.2355/isijinternational.ISIJINT-2017-696
[7] J. M. Milani, T. Saeid, Acicular ferrite nucleation and growth in API5L-X65 steel submerged arc welded joints, Mater. Sci. Technol. 36 (2020) 1398–1406. https://doi.org/10.1080/02670836.2020.1783774
[8] B. X. Wang, X. H Liu, G. D Wang, Inclusion characteristics and acicular ferrite nucleation in Ti-containing weld metals of X80 pipeline steel, Metall. Mater. Trans. A Phys. Metall. Mater. Sci. 49 (2018) 2124–2138. https://doi.org/10.1007/s11661-018-4570-y
[9] J. L. Lee, Y. T. Pan, The formation of intragranular acicular ferrite in simulated heat-affected zone, ISIJ Int. 35 (1995) 1027–1033. https://doi.org/10.2355/isijinternational.35.1027
[10] M. Ferrante, R. A. Farrar, The role of oxygen rich inclusions in determining the microstructure of weld metal deposits, J. Mater. Sci. 17 (1982) 3293–3298. https://doi.org/10.1007/BF01203498
[11] R. A. Farrar, P. L. Harrison, Acicular ferrite in carbon-manganese weld metals: An overview, J. Mater. Sci. 22 (1987) 3812–3820. https://doi.org/10.1007/BF01133327
[12] P. F. Chaveriat, G. S. Kim, S. Shah, J. E. Indacochea, Low carbon steel weld metal microstructures: The role of oxygen and manganese, J. Mater. Eng. 9 (1987) 253–267. https://doi.org/10.1007/BF02834145
[13] F. Han, B. Hwang, D. W. Suh, Z. C. Wang, D. L. Lee, S. J. Kim, Effect of molybdenum and chromium on hardenability of low-carbon boron-added steels, Met. Mater. Int. 14 (2008) 667–672. https://doi.org/10.3365/met.mat.2008.12.667
[14] N. Fujiyama, G. Shigesato, Effects of Mn and Al on acicular ferrite formation in SAW weld metal, ISIJ Int. 61 (2021) 1614–1622.https://doi.org/10.2355/isijinternational.ISIJINT-2020-407
[15] D. A. Mortimer, M. G. Nicholas, Surface and grain-boundary energies of AISI 316 stainless steel in the presence of boron, Met. Sci. 10 (1976) 326–332. https://doi.org/10.1179/msc.1976.10.9.326
[16] G. Shigesato, T. Fujishiro, T. Hara, Grain boundary segregation behavior of boron in low-alloy steel, Metall. Mater. Trans. A 45 (2014) 1876–1882. https://doi.org/10.1007/s11661-013-2155-3
[17] X. L. He, Y. Y. Chu, J. J. Jonas, Grain boundary segregation of boron during continuous cooling, Acta Metall. 37 (1989) 147–161. https://doi.org/10.1016/0001-6160(89)90274-5
[18] K. Seto, D. Larson, P. Warren, G. D. Smith, Grain boundary segregation in boron added interstitial free steels studied by 3-dimensional atom probe, Scripta Mater. 40 (1999) 1029–1034. https://doi.org/10.1016/S1359-6462(98)00485-0
[19] H. R. Lin, G. H. Cheng, Hardenability effect of boron on carbon steels, Mater. Sci. Technol. 3 (1987) 855–859. https://doi.org/10.1179/mst.1987.3.10.855
[20] A. Terzic, M. Calcagnotto, S. Guk, T. Schulz, R. Kawalla, Influence of boron on transformation behavior during continuous cooling of low alloyed steels, Mater. Sci. Eng. A 584 (2013) 32–40. https://doi.org/10.1016/j.msea.2013.07.010
[21] J. M. Dowling, J. M. Corbett, H. W. Kerr, Inclusion phases and the nucleation of acicular ferrite in submerged arc welds in high strength low alloy steels, Metall. Mater. Trans. A Phys. Metall. Mater. Sci. 17 (1986) 1611–1623. https://doi.org/10.1007/BF02650098
[22] D. J. Abson, Acicular ferrite and bainite in C-Mn and low alloy steel arc weld metals, Sci. Technol. Weld Join. 23 (2018) 635–648. https://doi.org/10.1080/13621718.2018.1461992
[23] R. A. Farrar, P. L. Harrison, Acicular ferrite in carbon manganese weld metals: An overview, J. Mater. Sci. 22 (1987) 3812–3820. https://doi.org/10.1007/BF01133327
[24] D. Liu, N. Guo, C. S. Xu, H. L. Li, K. Yang, J. C. Feng, Effects of Mo, Ti and B on microstructure and mechanical properties of underwater wet welding joints, J. Mater. Eng. Perform. 26 (2017) 2350–2358. https://doi.org/10.1007/s11665-017-2629-3
[25] W. Wang, Y. Y. Shan, K. Yang, Study of high strength pipeline steels with different microstructures, Mater. Sci. Eng. A 502 (2009) 38–44. https://doi.org/10.1016/j.msea.2008.10.042
[26] C. F. Wen, X. T. Deng, Y. Tian, Z. D. Wang, R. D. K. Misra, Microstructural evolution and toughness of the various HAZs in 1300-MPa-grade ultrahigh-strength structural steel, J. Mater. Eng. Perform. 28 (2019) 1301–1311. https://doi.org/10.1007/s11665-019-3869-1
[27] G. Spanos, M. G. Hall, The formation mechanism(s), morphology, crystallography of ferrite side plates, Metall. Mater. Trans. A Phys. Metall. Mater. 27 (1996) 1519–1534. https://doi.org/10.1007/BF02649812
[28] B. X. Wang, J. B. Lian, X. H. Liu, G. D. Wang, Effect of ultra-fast cooling on microstructure and mechanical properties in a plain low carbon steel, Kovove Mater. 52 (2014) 135–140. https://doi.org/10.4149/km_2014_3_135
[29] J. H. Chen, Y. Kikuta, T. Araki, M. Yoneda, Y. Matsuda, Micro-fracture behaviour induced by M-A constituent (Island Martensite) in simulated welding heat affected zone of HT80 high strength low alloyed steel, Acta Metall. 32 (1984) 1779–1788. https://doi.org/10.1016/0001-6160(84)90234-7
[30] C. L. Davis, J. E. King, Cleavage initiation in the intercritically reheated coarse-grained heat-affected zone: Part I. Fractographic evidence, Metall. Mater. Trans. A Phys. Metall. Mater. 25 (1994) 563–573. https://doi.org/10.1007/BF02651598
[31] J. C. F. Jorge, L. F. G. de Souza, M. C. Mendes, I. S. Bott, L. S. Araujo, V. R. dos Santos, J. M. A. Rebello, G. M. Evans, Microstructure characterization and its relationship with impact toughness of C-Mn and high strength low alloy steel weld metals – A review, J. Mater. Res. Technol. 10 (2021) 471–501. https://doi.org/10.1016/j.jmrt.2020.12.006
[32] S. Moeinifar, A. H. Kokabi, H. R. Madaah Hosseini, Role of tandem submerged arc welding thermal cycles

on properties of the heat affected zone in X80 microalloyed pipe line steel, J. Mater. Process. Technol. 211 (2011) 368–375. https://doi.org/10.1016/j.jmatprotec.2010.10.011

[33] J. J. Cui, W. T. Zhu, Z. Y. Chen, L. Q. Chen, Effect of simulated cooling time on microstructure and toughness of CGHAZ in novel high-strength low-carbon construction steel, Sci. Technol. Weld Join. 25 (2020) 169–177. https://doi.org/10.1080/13621718.2019.1661116

[34] H. Qin, Y. Guo, L. Wang, P. Liang, Y. Shi, Y. Cui, Effect of heat inputs on microstructure and mechanical properties in CGHAZ of BWELDY960Q steel, Kovove Mater. 57 (2019) 355–362. https://doi.org/10.4149/km_2019_5_355

[35] L. Y. Lan, C. L. Qiu, H. Y. Song, D. W. Zhao, Correlation of martensite-austenite constituent and cleavage crack initiation in welding heat affected zone of low carbon bainitic steel, Mater. Lett. 125 (2014) 86–88. https://doi.org/10.1016/j.matlet.2014.03.123

[36] C. W. Li, Y. Wang, Y. H. Chen, Influence of peak temperature during in-service welding of API X70 pipeline steels on microstructure and fracture energy of the reheated coarse grain heat-affected zones, J. Mater. Sci. 46 (2011) 6424–6431. https://doi.org/10.1007/s10853-011-5592-7

[37] L. Y. Lan, C. L. Qiu, D. W. Zhao, X. H. Gao, L. X. Du, Analysis of martensite-austenite constituent and its effect on toughness in submerged arc welded joint of low carbon bainitic steel, J. Mater. Sci. 47 (2012) 4732–4742. https://doi.org/10.1007/s10853-012-6346-x

[38] X. D. Li, Y. R. Fan, X. P. Ma, S. V. Subramanian, C. J. Shang, Influence of martensite-austenite constituents formed at different intercritical temperatures on toughness, Mater. Des. 67 (2015) 457–463. https://doi.org/10.1016/j.matdes.2014.10.028